



Growth of rock-salt MgO–NiO–ZnO films: Relationship between lattice constant and composition

Shintarou Iida, Takumi Ikenoue ^{*} , Masao Miyake, Tetsuji Hirato

Graduate School of Energy Science, Kyoto University, Yoshida-honmachi, Sakyo-ku, Kyoto 606-8501, Japan

ARTICLE INFO

Keywords:

Deep-ultraviolet light-emitting diode (DUV-LED)
Semiconductor
Oxide
Lattice matching
MgO
NiO
ZnO

ABSTRACT

Deep-ultraviolet light-emitting diodes (DUV-LEDs) have emerged as eco-friendly alternatives to mercury lamps for various applications. This study explores MgO–NiO–ZnO alloy semiconductors as potential materials for DUV-LEDs, offering advantages over conventional AlGaIn-based systems. MgO–NiO–ZnO films with varying compositions were grown using mist chemical vapor deposition (mist-CVD) and characterized using X-ray diffraction (XRD), scanning electron microscopy (SEM), energy-dispersive X-ray (EDX) spectroscopy, and UV–visible spectroscopy. A single-phase rock-salt structure was obtained for ZnO mole fractions of up to 0.26, whereas phase separation occurred at higher levels of ZnO content. The lattice constant–composition relationship followed Vegard's law, suggesting that MgO–NiO–ZnO films with a composition of $Mg_x(Ni_{0.67}Zn_{0.33})_{1-x}O$ could achieve lattice matching with MgO substrates. The band gaps of rock-salt MgO–NiO–ZnO, determined based on spectral transmittance measurements, ranged from 5.4 eV to 5.8 eV and increased with MgO content. These band gap values are sufficient for DUV-LED applications. This study provides crucial insights into MgO–NiO–ZnO alloy semiconductors, paving the way for the development of more efficient and strain-free DUV-LEDs.

1. Introduction

Deep-ultraviolet (DUV) light-emitting diodes (LEDs) are being developed as an environmentally friendly alternative to mercury fluorescent lamps for applications in the medical, water purification, and public health sectors [1–3]. DUV-LEDs offer strong sterilization power without the environmental hazards associated with mercury. Currently, AlGaIn, an alloy of AlN (6.2 eV) [4–6] and GaN (3.4 eV) [6,7], is one of the most studied semiconductors for DUV-LED light-emitting layers. Various AlGaIn-based (D)UV-LEDs have been developed [8–10]. The band gap of AlGaIn can be controlled by adjusting the AlN ratio. However, owing to the significant difference between the lattice constants of AlN and GaN, epitaxial strain inevitably occurs in layered structures of DUV-LEDs, which consist of layers with different compositions and lattice constants [11].

To address this challenge, we are focusing on a MgO–NiO–ZnO alloy semiconductor that could potentially be lattice-matched with MgO substrates. MgO and NiO both have rock-salt crystal structures, which have a small lattice mismatch of 0.84 % [12–14]. Similarly, ZnO also has a metastable rock-salt structure, which occurs in addition to its stable wurtzite structure [15,16]. The MgO–NiO–ZnO system shows promise

for several reasons: First, it has less lattice mismatch compared to those exhibited by other alloy systems such as AlInGaIn and α -(AlInGa)₂O₃ [11,17]. Less lattice mismatch is illustrated by narrower widths for the triangles for each alloy system in Fig. 1, which shows the average bond lengths and band gaps of various semiconductors [4–7,11,17–21] and MgO–NiO–ZnO [12–17,22–25]. Second, it has a potential for lattice matching with MgO substrates at appropriate NiO:ZnO ratios. Finally, it allows for a large and wide control of the band gap while maintaining lattice matching. The difficulty in achieving this characteristic with substrates such as AlN, GaN, and α -Al₂O₃ is illustrated by the non-acuteness of the triangles representing these alloy systems in Fig. 1. The band gap of MgO (7.8 eV) [12,22,23] is significantly larger than those of NiO (3.7–3.8 eV) [12,24] and rock-salt ZnO (2.4 eV) [15]. Through increases in the MgO content, the band gap of MgO–NiO–ZnO can be enlarged. Notably, when the NiO:ZnO ratio is optimized to match the lattice constant of MgO, the lattice constant remains unchanged even as the MgO composition is adjusted to control the band gap. This unique property suggests that the band gaps of MgO–NiO–ZnO alloy semiconductors could potentially be changed from approximately 3.0 eV to 7.8 eV, while lattice matching is maintained with an MgO substrate. The maximum band gap of 7.8 eV is sufficient for fabricating DUV-LEDs that

^{*} Correspondence to: Graduate School of Energy Science, Kyoto University, Kyoto 606-8501, Japan.

E-mail address: ikenoue.takumi.4m@kyoto-u.ac.jp (T. Ikenoue).

<https://doi.org/10.1016/j.jalcom.2025.179272>

Received 13 December 2024; Received in revised form 12 February 2025; Accepted 17 February 2025

Available online 18 February 2025

0925-8388/© 2025 The Authors. Published by Elsevier B.V. This is an open access article under the CC BY-NC-ND license (<http://creativecommons.org/licenses/by-nc-nd/4.0/>).

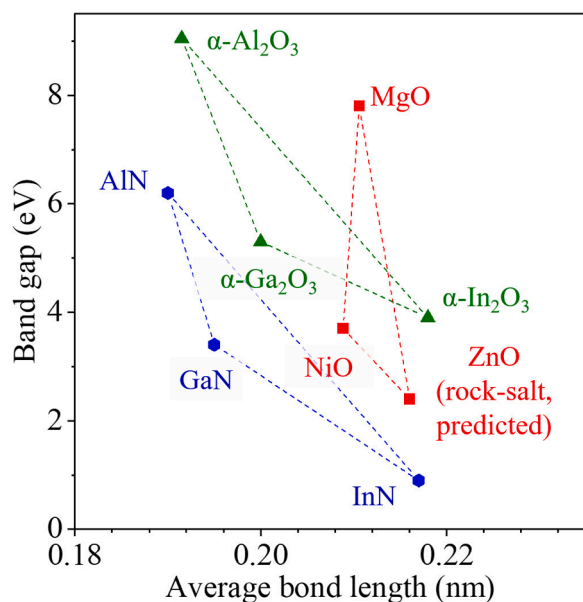


Fig. 1. Average bond lengths and band gaps of various semiconductors [4–7, 11,17–21] and MgO–NiO–ZnO [12–17,22–25].

emit light at wavelengths of approximately 160 nm.

However, the exact relationship between the lattice constant and composition of rock-salt MgO–NiO–ZnO, in conjunction with the precise lattice-matching composition, has not been fully determined. In this study, we investigated the relationship between the lattice constant and composition of rock-salt MgO–NiO–ZnO. MgO–NiO–ZnO films of various compositions were deposited using mist chemical vapor deposition (mist-CVD). These films were then analyzed to determine their lattice constants, compositions, and band gaps. This study aims to provide crucial insights into the properties of MgO–NiO–ZnO alloy semiconductors, potentially paving the way for the development of more

efficient and strain-free DUV-LEDs. This study represents an important step toward creating environmentally friendly, high-performance DUV light sources that could significantly impact various fields, including medical applications, water treatment, and public health.

2. Experiment

MgO–NiO–ZnO films were grown via mist-CVD using the setup shown in Fig. 2. The precursor Mg, Ni, and Zn solutions were aqueous solutions of their respective acetylacetonate salts. To enhance solubility, ethylenediamine and hydrochloric acid were added to the Ni and Zn precursor solutions, respectively. The standard concentrations were 0.02 M for the precursors and 0.04 M for the additives. The precursor solutions were poured into misting bottles with polymer film-wrapped bottoms and atomized using ultrasonic waves generated by piezoelectric elements (HM-2412, Honda Electronics). The mists of the precursor solutions were carried by carrier gases and mixed in a mist-mixing bottle. Dry air was used as the carrier and dilution gas. The flow rate of the dilution gas was set to 2 L·min⁻¹, and the total flow rate of all the carrier gases was set to 4 L·min⁻¹. The film composition was controlled by adjusting the carrier-gas ratios or diluting the precursor solutions. A rubber heater maintained at 90°C enveloped the quartz tube inlet to prevent mist condensation. The quartz tube was heated in an electric furnace (ARF-50KC, Asahi-rika), with the substrates maintained at 600°C. To investigate the lattice constants independent of strain effects, the MgO–NiO–ZnO films were grown on quartz substrates (25 × 25 × 0.7 mm, Mitorika).

X-ray diffraction (XRD) (X'pert PRO MPD, Malvern PANalytical) was used to determine the crystal structures and lattice constants of the films. The surface morphology was examined using scanning electron microscopy (SEM) (JSM-6510LV, Jeol), whereas the film composition was analyzed via energy-dispersive X-ray (EDX) spectroscopy integrated with SEM. The optical bandgaps were derived from transmittance measurements obtained via UV–visible spectroscopy (UV-1900i, Shimadzu Corporation).

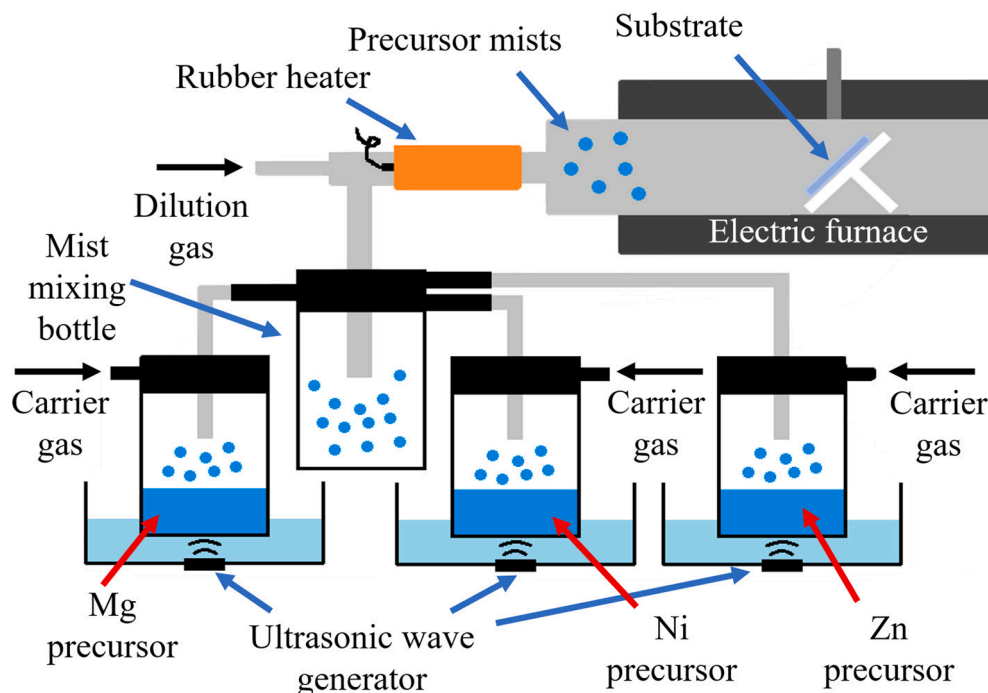


Fig. 2. Schematic of mist-CVD setup.

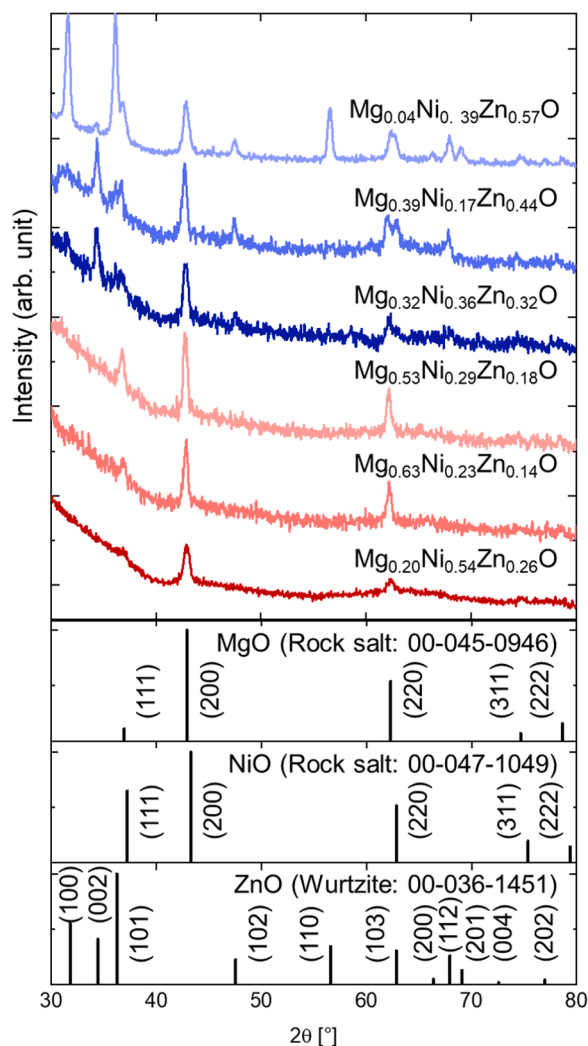


Fig. 3. XRD 2θ scans of representative MgNiZnO films.

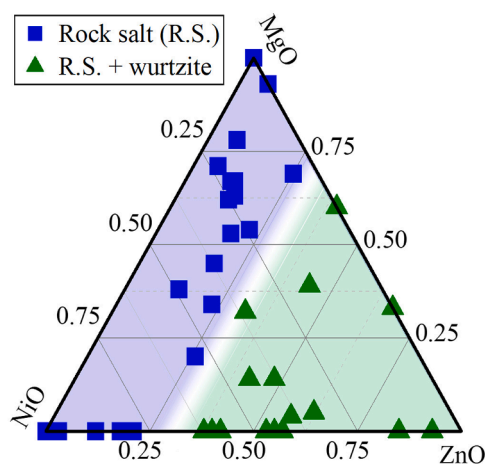


Fig. 4. Crystal phases and compositions of obtained MgO–NiO–ZnO films.

3. Results

XRD 2θ scans and EDX were conducted on all 36 deposited MgO–NiO–ZnO films to analyze their structures and compositions, respectively. Fig. 3 shows XRD 2θ scans of two typical films. $\text{Mg}_{0.20}\text{Ni}_{0.54}\text{Zn}_{0.26}\text{O}$ (blue line in Fig. 3) represents the films in which the ZnO mole fraction, $[\text{ZnO}]$, is 0.26 or less. For these films, only XRD patterns attributable to MgO–NiO, the rock-salt-structure crystals, were detected. Thus, these films exhibit a single-phase rock-salt crystal structure. On the other hand, $\text{Mg}_{0.32}\text{Ni}_{0.36}\text{Zn}_{0.32}\text{O}$ (red line in Fig. 3), representing the films in which $[\text{ZnO}]$ is 0.32 or more, demonstrated not only a rock-salt structure but also a wurtzite structure. These results indicate that the films with $[\text{ZnO}] \geq 0.32$ are phase separated into wurtzite and rock-salt structures. Fig. 4 shows the relationship between the crystal phases and compositions of the MgO–NiO–ZnO films. The MgO–NiO–ZnO films were divided into two groups: those with a single-phase rock-salt structure, where $[\text{ZnO}] \leq 0.26$, which are represented by the blue squares; and those phase-separated into rock-salt and wurtzite structures, where $[\text{ZnO}] \geq 0.32$, which are represented by the green triangles. Fig. 5 shows surface SEM images of $\text{Mg}_{0.20}\text{Ni}_{0.54}\text{Zn}_{0.26}\text{O}$ and $\text{Mg}_{0.32}\text{Ni}_{0.36}\text{Zn}_{0.32}\text{O}$. The films with single-phase rock-salt structures had flat surfaces, whereas those with phase separation had many grains. The bright grains may be wurtzite-structured crystals.

The lattice constants of the rock-salt MgO–NiO–ZnO were evaluated based on the Bragg angles. For each sample, the lattice constants were calculated based on five peaks of the rock-salt phase, namely, (111), (200), (220), (311), and (222). The analytical error in the lattice constants obtained based on these five peaks had a maximum value of 0.00005 nm, indicating sufficient accuracy. Because it is not easy to evaluate the compositions of phase-separated films, only the single-phase rock-salt films were analyzed. Fig. 6 shows the relationship between the lattice constants and compositions as derived via this analysis. It can be observed that the lattice constants of the MgO–NiO–ZnO films varied in a regular manner with respect to the composition. Additionally, the occurrence of films with high ZnO content exhibiting lattice constants larger than that of MgO provides supporting evidence for the possibility of attaining lattice matching between MgO substrates and MgO–NiO–ZnO alloys at specific compositional ratios. These measurement results appear to follow Vegard's law, which indicates a linear relationship between the lattice constant and composition, given that the data points are distributed on a plane. Therefore, applying Vegard's law, the relationship between the lattice constant and composition of MgO–NiO–ZnO can be expressed by the following equation, where the lattice constants of MgO and NiO are 0.4212 nm and 0.4177 nm, respectively [10]:

$$a(\text{nm}) = 0.4212[\text{MgO}] + 0.4177[\text{NiO}] + 0.4282[\text{ZnO}], \quad (1)$$

where $[\text{MgO}]$, $[\text{NiO}]$, and $[\text{ZnO}]$ are the molar fractions of MgO, NiO, and ZnO, respectively, in MgO–NiO–ZnO. Considering the error of approximation, the lattice constant of rock-salt ZnO is determined to be 0.4282 ± 0.0005 nm. This lattice constant value, 0.4282 nm, agreed with the lattice constant calculated from the ionic radii of Zn^{2+} and O^{2-} [17]. Considering the value of the approximation error, it is inferred that these evaluations have been performed accurately within the precision of errors derived from the measurement capabilities of XRD and EDX. The composition that results in a lattice constant matching that of MgO is $[\text{ZnO}]/([\text{NiO}] + [\text{ZnO}]) = 0.33$, regardless of $[\text{MgO}]$. Based on the phase diagram shown in Fig. 4, $\text{Mg}_x(\text{Ni}_{0.67}\text{Zn}_{0.33})\text{O}$ is expected to maintain a single-phase rock-salt structure over a wide $[\text{MgO}]$ range.

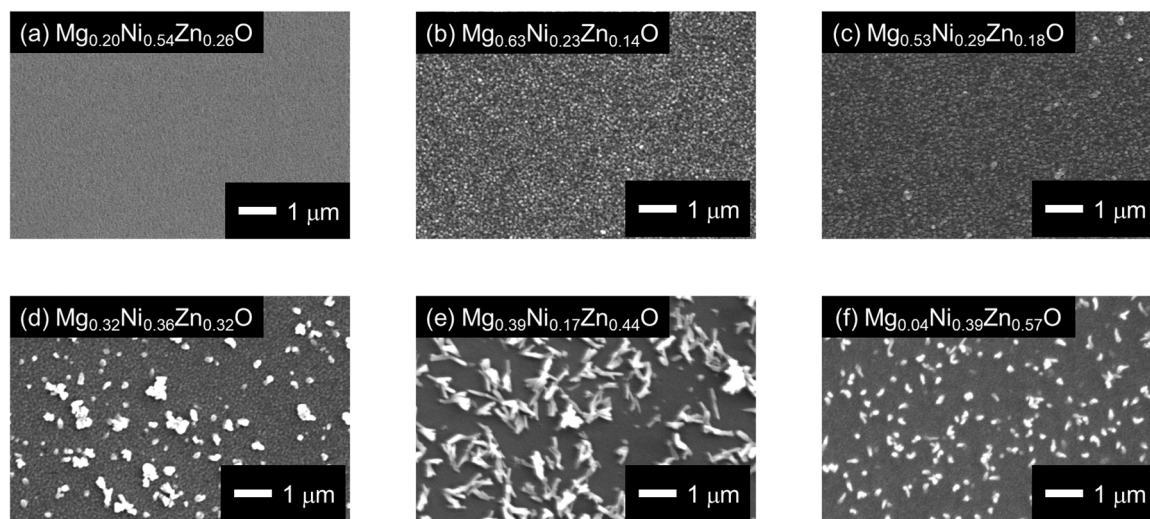


Fig. 5. Surface SEM images of (a) $\text{Mg}_{0.20}\text{Ni}_{0.54}\text{Zn}_{0.26}\text{O}$, (b) $\text{Mg}_{0.63}\text{Ni}_{0.23}\text{Zn}_{0.14}\text{O}$, (c) $\text{Mg}_{0.53}\text{Ni}_{0.29}\text{Zn}_{0.18}\text{O}$, (d) $\text{Mg}_{0.32}\text{Ni}_{0.36}\text{Zn}_{0.32}\text{O}$, (e) $\text{Mg}_{0.39}\text{Ni}_{0.17}\text{Zn}_{0.44}\text{O}$, and (f) $\text{Mg}_{0.04}\text{Ni}_{0.39}\text{Zn}_{0.57}\text{O}$.

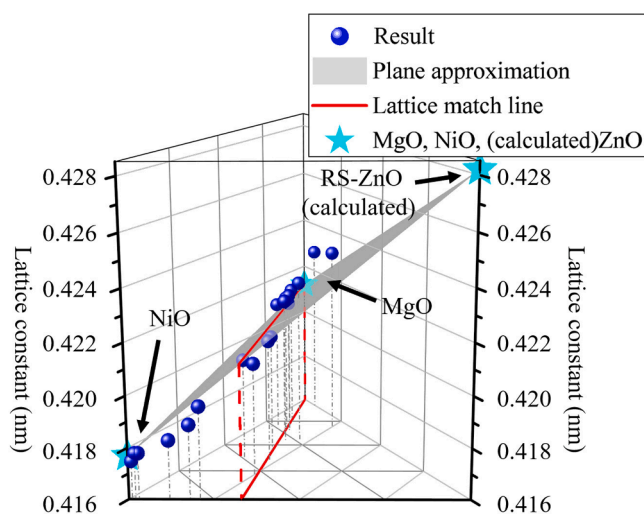


Fig. 6. Relationship between lattice constant and composition of rock-salt MgO-NiO-ZnO.

There is a high probability that even $\text{Ni}_{0.67}\text{Zn}_{0.33}\text{O}$, which does not contain MgO, could grow as a single-phase rock-salt structure on MgO substrates.

The band gaps of the MgO-NiO-ZnO thin films were evaluated based on the measured optical transmittance spectra. Fig. 7(a) presents a ternary composition diagram illustrating the relationship between the band gap and composition of the MgO-NiO-ZnO films. The band gap values are represented by color gradients. Continuous color mapping was generated via the smoothing and extrapolation of the data obtained at the compositions indicated by the black squares in the figure. The variation in band gap across the composition space is visualized clearly

by the transition from the blue to red regions, indicating the dominant role of MgO content in determining the band gap: the band gap increases from 5.4 to 5.8 eV with increasing MgO content. Fig. 7(b) compares the band gap values of the MgO-NiO-ZnO system (red stars) with those previously reported for binary MgO-ZnO systems (other symbols) [15, 22,26–29]. The band gap shows a consistent upward trend with increasing MgO content, ranging from approximately 4.5 eV to 7.5 eV. Notably, the band gap values of the ternary MgO-NiO-ZnO system aligns well with those reported for binary MgO-ZnO, following a similar compositional dependence. These results indicate that the band gap of the MgO-NiO-ZnO system is determined primarily by the MgO content.

4. Conclusion

This study investigated the composition-dependent properties of grown MgO-NiO-ZnO alloy films for potential use in deep-ultraviolet light-emitting diodes. A single-phase rock-salt structure was obtained for compositions with ZnO molar ratios of up to 0.26, whereas a higher ZnO content led to phase separation. The lattice constant a of the rock-salt MgO-NiO-ZnO was calculated using the following equation: $a(\text{nm}) = 0.4212[\text{MgO}] + 0.4177[\text{NiO}] + 0.4282[\text{ZnO}]$, where $[\text{MgO}]$, $[\text{NiO}]$, and $[\text{ZnO}]$ are the levels of MgO, NiO, and ZnO content, respectively. Importantly, the composition $\text{Mg}_x(\text{Ni}_{0.67}\text{Zn}_{0.33})_{1-x}\text{O}$ was identified to be potentially lattice-matched to MgO substrates across all MgO compositions. The band gap of rock-salt MgO-NiO-ZnO was 5.4–5.8 eV and increased as MgO content increased. These findings suggest that MgO-NiO-ZnO alloys offer promising characteristics for DUV-LED applications, including the potential for lattice matching with MgO substrates and tunable band gaps. Future research prospects include growing lattice-matched MgO-NiO-ZnO on MgO substrates and evaluating the optical properties and both p- and n-type doping for DUV-LED applications.

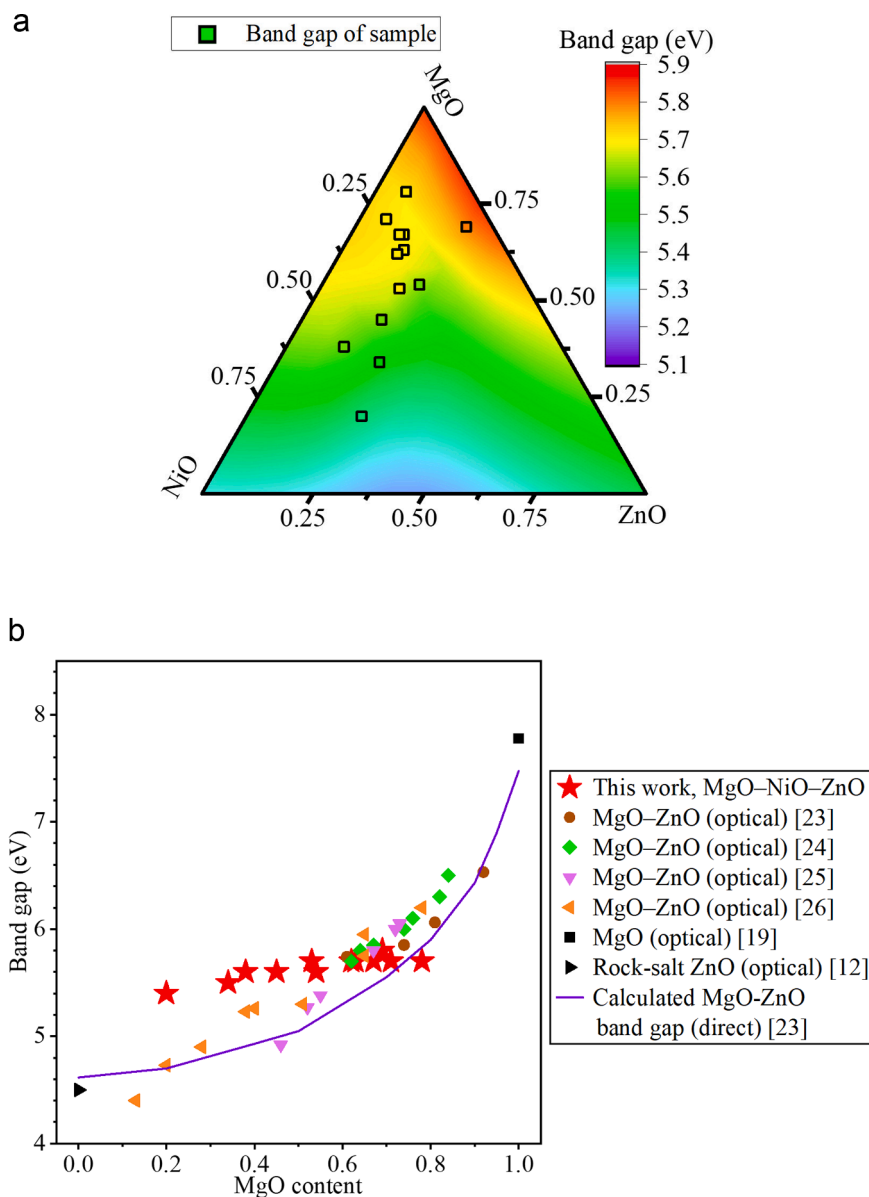


Fig. 7. (a) Ternary composition diagram showing band gaps of MgO–NiO–ZnO films. Band gaps were evaluated using Tauc plots from the UV–vis spectrum and are indicated by black squares. Color map shows band gaps across entire composition range, calculated through interpolation, extrapolation, and smoothing of these experimental data. Relationship between band gap values and colors is shown in color scale. (b) Correlation between band gap values and MgO content for MgO–NiO–ZnO films (red stars) compared with previously reported data for MgO–ZnO systems [15,22,26–29]. Purple line represents calculated band gap values for direct transitions in MgO–ZnO [26].

CRediT authorship contribution statement

Hirato Tetsuji: Writing – review & editing, Supervision. **Miyake Masao:** Writing – review & editing, Supervision. **Ikenoue Takumi:** Writing – review & editing, Writing – original draft, Visualization, Validation, Resources, Project administration, Methodology, Investigation, Funding acquisition, Formal analysis, Conceptualization. **Iida Shintarou:** Writing – review & editing, Writing – original draft, Visualization, Validation, Methodology, Investigation, Formal analysis, Data curation.

Declaration of Generative AI and AI-assisted technologies in the writing process

During the preparation of this work, Shintarou Iida used Copilot and Gemini to improve the readability of the draft. After using this tool/

service, Shintarou Iida reviewed and edited the content as needed and is taking full responsibility for the content of the published article.

Declaration of Competing interest

The authors declare that they have no known competing financial interests or personal relationships that could have appeared to influence the work reported in this paper

Acknowledgements

This work was supported by JST SPRING Grant Number JPMJSP2110, JSPS KAKENHI Grant-in-Aid for Scientific Research C Grant Number 20K04580, and JSPS Fostering Joint International Research A Grant Number 21KK0260.

Data availability

Data will be made available on request.

References

- [1] D. Welch, M. Buonanno, V. Grilj, I. Shuryak, C. Crickmore, A.W. Bigelow, G. Randers-Pehrson, G.W. Johnson, D.J. Brenner, Far-UVC light: a new tool to control the spread of airborne-mediated microbial diseases, *Sci. Rep.* 8 (2018) 2752, <https://doi.org/10.1038/s41598-018-21058-w>.
- [2] M. Buonanno, D. Welch, I. Shuryak, D.J. Brenner, Far-UVC light (222 nm) efficiently and safely inactivates airborne human coronaviruses, *Sci. Rep.* 10 (2020) 10285, <https://doi.org/10.1038/s41598-020-67211-2>.
- [3] W. Kowalski, *Ultraviolet Germicidal Irradiation Handbook: UVGI for Air and Surface Disinfection*, first ed., Springer, Berlin, Heidelberg, 2010 <https://doi.org/10.1007/978-3-642-01999-9>.
- [4] W.M. Yim, E.J. Stofko, P.J. Zanzucchi, J.I. Pankove, M. Ettenberg, S.L. Gilbert, Epitaxially grown AlN and its optical band gap, *J. Appl. Phys.* 44 (1973) 292–296, <https://doi.org/10.1063/1.1661876>.
- [5] P.B. Perry, R.F. Rutz, The optical absorption edge of single-crystal AlN prepared by a close-spaced vapor process, *Appl. Phys. Lett.* 33 (1978) 319–321, <https://doi.org/10.1063/1.90354>.
- [6] S.R. Lee, A.F. Wright, M.H. Crawford, G.A. Petersen, J. Han, R.M. Biefeld, The band-gap bowing of $\text{Al}_x\text{Ga}_{1-x}\text{N}$ alloys, *Appl. Phys. Lett.* 74 (1999) 3344–3346, <https://doi.org/10.1063/1.123339>.
- [7] B. Monemar, Fundamental energy gap of GaN from photoluminescence excitation spectra, *Phys. Rev. B* 10 (1974) 676–681, <https://doi.org/10.1103/PhysRevB.10.676>.
- [8] H. Yu, M.H. Memon, D. Wang, Z. Ren, H. Zhang, C. Huang, M. Tian, H. Sun, S. Long, AlGaIn-based deep ultraviolet micro-LED emitting at 275 nm, *Opt. Lett.* 46 (2021) 3271, <https://doi.org/10.1364/ol.431933>.
- [9] M.H. Memon, H. Yu, Y. Luo, Y. Kang, W. Chen, D. Li, D. Luo, S. Xiao, C. Zuo, C. Gong, C. Shen, L. Fu, B.S. Ooi, S. Liu, H. Sun, A three-terminal light emitting and detecting diode, *Nat. Electron.* 7 (2024) 279–287, <https://doi.org/10.1038/s41928-024-01142-y>.
- [10] H. Sun, S. Mitra, R.C. Subedi, Y. Zhang, W. Guo, J. Ye, M.K. Shakfa, T.K. Ng, B. S. Ooi, I.S. Roqan, Z. Zhang, J. Dai, C. Chen, S. Long, Unambiguously enhanced ultraviolet luminescence of algan wavy quantum well structures grown on large misoriented sapphire substrate, *Adv. Funct. Mater.* 29 (2019), <https://doi.org/10.1002/adfm.201905445>.
- [11] A.F. Wright, J.S. Nelson, Consistent structural properties for AlN, GaN, and InN, *Phys. Rev. B* 51 (1995) 7866–7869, <https://doi.org/10.1103/PhysRevB.51.7866>.
- [12] C.A. Niedermeier, M. Räsander, S. Rhode, V. Kachkanov, B. Zou, N. Alford, M. A. Moram, Band gap bowing in $\text{Ni}_x\text{Mg}_{1-x}\text{O}$, *Sci. Rep.* 6 (2016) 31230, <https://doi.org/10.1038/srep31230>.
- [13] A. Kuzmin, N. Mironova, Composition dependence of the lattice parameter in $\text{Ni}_x\text{Mg}_{1-x}\text{O}$ solid solutions, *J. Phys. Condens. Matter* 10 (1998) 7937–7944, <https://doi.org/10.1088/0953-8984/10/36/004>.
- [14] R.L. Clendenen, H.G. Drickamer, Lattice parameters of nine oxides and sulfides as a function of pressure, *J. Chem. Phys.* 44 (1966) 4223–4228, <https://doi.org/10.1063/1.1726610>.
- [15] A. Segura, J.A. Sans, F.J. Manjón, A. Muñoz, M.J. Herrera-Cabrera, Optical properties and electronic structure of rock-salt ZnO under pressure, *Appl. Phys. Lett.* 83 (2003) 278–280, <https://doi.org/10.1063/1.1591995>.
- [16] C.H. Bates, W.B. White, R. Roy, New high-pressure polymorph of zinc oxide, *Science* 137 (1962) 993, <https://doi.org/10.1126/science.137.3534.993.a>.
- [17] R.D. Shannon, Revised effective ionic radii and systematic studies of interatomic distances in halides and chalcogenides, *Acta Cryst. A* 32 (1976) 751–767, <https://doi.org/10.1107/S0567739476001551>.
- [18] V.Y. Davydov, A.A. Klochikhin, R.P. Seisyan, V.V. Emtsev, S.V. Ivanov, F. Bechstedt, J. Furthmüller, H. Harima, A.V. Mudryi, J. Aderhold, O. Semchinova, J. Graul, Absorption and emission of hexagonal InN. Evidence of narrow fundamental band gap, *Phys. Stat. Sol. (b)* 229 (2002) R1–R3, [https://doi.org/10.1002/1521-3951\(200202\)229:3%3CR1::AID-PSSB99991%3E3.0.CO;2-O](https://doi.org/10.1002/1521-3951(200202)229:3%3CR1::AID-PSSB99991%3E3.0.CO;2-O).
- [19] R.H. French, Electronic band structure of Al_2O_3 , with comparison to Alon and AlN, *J. Am. Ceram. Soc.* 73 (1990) 477–489, <https://doi.org/10.1111/j.1151-2916.1990.tb06541.x>.
- [20] H. Nishinaka, D. Tahara, S. Morimoto, M. Yoshimoto, Epitaxial growth of $\alpha\text{-Ga}_2\text{O}_3$ thin films on a-, m-, and r-plane sapphire substrates by mist chemical vapor deposition using $\alpha\text{-Fe}_2\text{O}_3$ buffer layers, *Mater. Lett.* 205 (2017) 28–31, <https://doi.org/10.1016/j.matlet.2017.06.003>.
- [21] P.D.C. King, T.D. Veal, F. Fuchs, C.Y. Wang, D.J. Payne, A. Bourlange, H. Zhang, G. R. Bell, V. Cimalla, O. Ambacher, R.G. Egdel, F. Bechstedt, C.F. McConville, Band gap, electronic structure, and surface electron accumulation of cubic and rhombohedral In_2O_3 , *Phys. Rev. B Condens. Matter Mater. Phys.* 79 (2009) 205211, <https://doi.org/10.1103/PhysRevB.79.205211>.
- [22] R.C. Whited, W.C. Walker, Exciton spectra of CaO and MgO, *Phys. Rev. Lett.* 22 (1969) 1428–1430, <https://doi.org/10.1103/PhysRevLett.22.1428>.
- [23] D.M. Roessler, W.C. Walker, Electronic spectrum and ultraviolet optical properties of crystalline MgO, *Phys. Rev.* 159 (1967) 733–738, <https://doi.org/10.1103/PhysRev.159.733>.
- [24] H. Sato, T. Minami, S. Takata, T. Yamada, Transparent conducting p-type NiO thin films prepared by magnetron sputtering, *Thin Solid Films* 236 (1993) 27–31, [https://doi.org/10.1016/0040-6090\(93\)90636-4](https://doi.org/10.1016/0040-6090(93)90636-4).
- [25] A. JemmyCinthia, G. Sudhapriyang, R. Rajeswarapalanichamy, M. Santhosh, Structural, electronic and elastic properties of ZnO and CdO: a first-principles study, *Procedia Mater. Sci.* 5 (2014) 1034–1042, <https://doi.org/10.1016/j.mspro.2014.07.394>.
- [26] T. Onuma, M. Ono, K. Ishii, K. Kaneko, T. Yamaguchi, S. Fujita, T. Honda, Impact of local arrangement of Mg and Zn atoms in rocksalt-structured $\text{Mg}_x\text{Zn}_{1-x}\text{O}$ alloys on bandgap and deep UV cathodoluminescence peak energies, *Appl. Phys. Lett.* 113 (2018) 061903, <https://doi.org/10.1063/1.5031174>.
- [27] I. Takeuchi, W. Yang, K.S. Chang, M.A. Aronova, T. Venkatesan, R.D. Vispute, L. A. Bendersky, Monolithic multichannel ultraviolet detector arrays and continuous phase evolution in $\text{Mg}_x\text{Zn}_{1-x}\text{O}$ composition spreads, *J. Appl. Phys.* 94 (2003) 7336–7340, <https://doi.org/10.1063/1.1623923>.
- [28] S. Chooapun, R.D. Vispute, W. Yang, R.P. Sharma, T. Venkatesan, H. Shen, Realization of band gap above 5.0 eV in metastable cubic-phase $\text{Mg}_x\text{Zn}_{1-x}\text{O}$ alloy films, *Appl. Phys. Lett.* 80 (2002) 1529–1531, <https://doi.org/10.1063/1.1456266>.
- [29] M.C. Wen, S.A. Lu, L. Chang, M.M.C. Chou, K.H. Ploog, Epitaxial growth of rocksalt $\text{Zn}_{1-x}\text{Mg}_x\text{O}$ on MgO (100) substrate by molecular beam epitaxy, *J. Cryst. Growth* 477 (2017) 169–173, <https://doi.org/10.1016/j.jcrysgro.2017.01.023>.